Electronic Supplementary Material (ESI) for Journal of Materials Chemistry A.

Electronic supplementary information

The roles of oxygen vacancies, electrolyte composition, lattice structure, and doping density on the electrochemical reactivity of Magnéli phase TiO_2 anodes

Yin Jing,[a] Soroush Almassi,[a] Shafigh, Mehraeen,[a] Robert LeSuer,[b] Brian P. Chaplin[a*]

[a] *Department of Chemical Engineering, University of Illinois at Chicago, 810 South Clinton Street, Chicago, Illinois 60607, United States*

[b] *Department of Chemistry, The College at Brockport, State University of New York, Brockport, New York 14420, United States*

[*] *Corresponding author. Phone: (+1)312-996-0288; Fax: (+1)312-996-0808; E-mail: chaplin@uic.edu.*

S-1. Supplementary Methods

Experimental Apparatus. The marked pattern was examined by using a nano-contour GT-K optical profilometer (Bruker, Billerica, Massachusetts). The crystalline structures of Ti_nO_{2n-1} were examined by X-ray diffraction (Siemens D-5000) with a Cu X-ray tube (40 kV and 25 mA), and scans were collected with DataScan software (MDI, v. 4.3.355, 2005) at a 0.02° step size and a 0.6 s dwell time, XRD patterns were examined in MDI Jade Plus v 6.5.26. The surface elemental composition of Ti_nO_{2n-1} was examined by X-ray photoelectron spectroscopy (XPS, Kratos, Axis-165), XPS spectra were adjusted according to the standard peak position of carbon at 284.5 eV, and XPS peak fitting was implemented on XPS Peak Software V 4.1. The film resistance was measured through a source meter (Keithley 2615) using a two-point probe method.

Accurate Positioning on Ti_nO_{2n-1} Electrode and Laser Marking. To study the local kinetics in different electrode states, 5 random and well separated marker points were picked from the electrode surface, and a circular area of 80-micron diameter was studied using each marker point as the center of the circle. To accurately position the UME to the same spots of interest among different experiments, a triangulation scheme was adopted, which determined the location of the marker point by measuring the distance from the three anchor points. Briefly, the relative distances of one marker point to the three anchor points were recorded in the first experiment, and a new coordinate of that specific point in later experiments was calculated by satisfying these relative distances. The marked pattern, as shown in Figure S-8, was examined by using the profilometer, and it was confirmed that the laser at this configuration was able to make a trench with a 40 μm depth determined by the profilometer. A comparison of the images collected by the profilometer and SECM was shown in *SI Section S-9*.

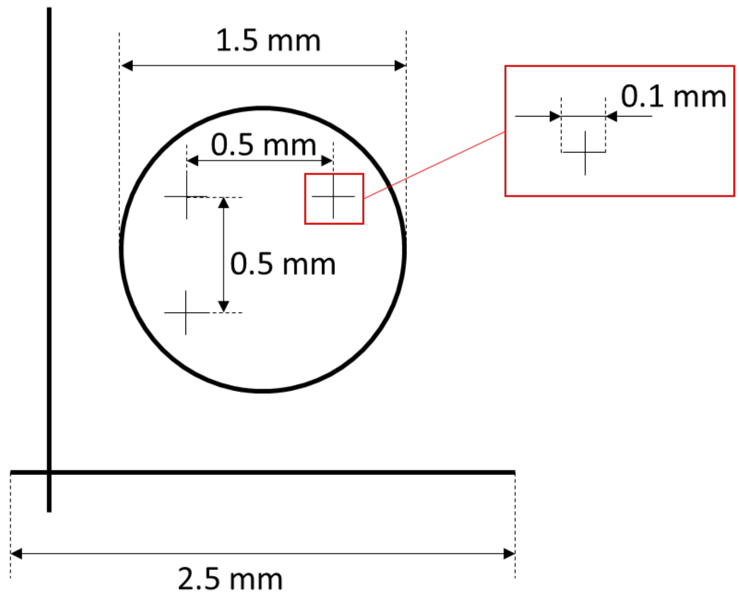

Figure S-1 Laser marking pattern drawing

S-2. Cyclic Voltammogram on SECM UME in 5 mM RuHex and 100 mM KCl

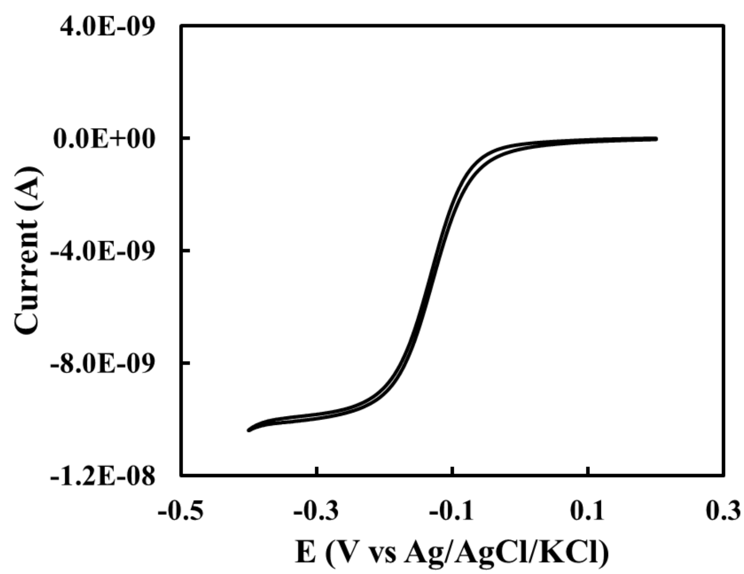

Figure S-2 Cyclic voltammogram on a Pt UME with 10-micron diameter in 5 mM Ru[III]Hex and 100 mM KCl, scan rate: 0.05 V s^{-1}.

S-3. Justification of Topographic Mapping Using Oxygen Reduction Reaction on Ti_nO_{2n-1}

The probe approach curve from the bulk solution to the unbiased Ti_nO_{2n-1} (open circuit potential 0.32 V vs SHE) substrate exhibited negative feedback, indicating that the unbiased substrate is not electrochemical active for the oxygen reduction reaction. Cyclic voltammetry results, as shown in the Figure S-3, also showed that the potential required to drive oxygen reduction reaction at Ti_nO_{2n-1} substrate is -0.80 V, so that the unbiased substrate (0.32 V vs SHE) would have little impact on the tip current when it was used for oxygen reduction.

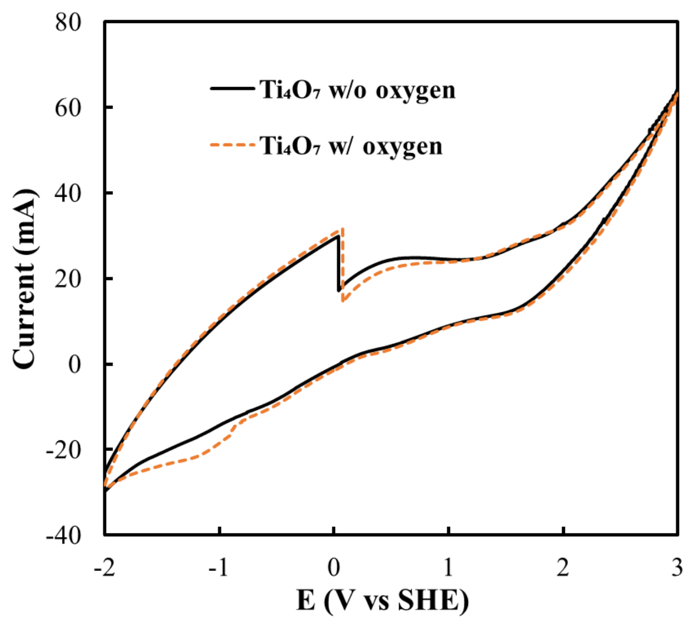

Figure S-3 Cyclic voltammogram of Ti_nO_{2n-1} electrode in 1 M $NaClO_4$ aerated solution (solid blank line) and argon purged solution (dashed orange line), scan rate: 0.1 V s^{-1}.

S-4. Estimated Crystal Size and Lattice Strain from the XRD

Table S-1 Estimated crystal sizes and lattice strains from the XRD of Ti_nO_{2n-1} studied in H_2SO_4 electrolyte

Peak	Pristine		Anodic Ageing		30 min Cathodic Reactivation		120-min cathodic Reactivation	
	Crystal Size (nm)	Lattice Strain (%)	Crystal Size (nm)	Lattice Strain (%)	Crystal Size (nm)	Lattice Strain (%)	Crystal Size (nm)	Lattice Strain (%)
20.76	97	1.99	95	1.99	97	1.99	102	1.20
26.37	83	1.84	80	1.63	86	1.87	85	1.85
29.58	82	1.67	85	1.82	78	1.53	80	1.58
31.74	110	1.15	105	1.10	107	1.13	112	1.17
34.08	86	1.38	80	1.21	88	1.42	85	1.34
Mean	92	1.60	89	1.55	91	1.59	93	1.43
Error	10	0.30	10	0.34	10	0.30	12	0.25

Table S-2 Estimated crystal sizes and lattice strains from the XRD of Ti_nO_{2n-1} studied in $HClO_4$ electrolyte

Peak	Pristine		Anodic Ageing		30 min Cathodic Reactivation	
	Crystal Size (nm)	Lattice Strain (%)	Crystal Size (nm)	Lattice Strain (%)	Crystal Size (nm)	Lattice Strain (%)
20.76	73	2.66	79	2.79	82	2.87
26.37	76	2.02	71	1.88	80	2.81
29.58	83	1.64	86	1.69	86	1.69
31.74	80	1.59	88	1.65	85	1.60
34.08	85	1.39	78	1.23	80	1.25
Mean	79	1.86	80	1.85	83	2.04
Error	4	0.44	6	0.51	2	0.65

Table S-3 Estimated crystal sizes and lattice strains from the XRD of Ti_nO_{2n-1} studied in HClO electrolyte

Peak	Pristine		Anodic Ageing		30 min Cathodic Reactivation	
	Crystal Size (nm)	Lattice Strain (%)	Crystal Size (nm)	Lattice Strain (%)	Crystal Size (nm)	Lattice Strain (%)
20.76	100	1.92	95	1.87	110	1.98
26.37	78	1.95	75	1.88	78	1.95
29.58	129	1.05	119	0.94	125	1.02
31.74	81	1.56	87	1.67	78	1.50
34.08	128	0.93	125	0.89	123	0.81
Mean	103	1.48	100	1.45	103	1.45
Error	22	0.42	19	0.43	20	0.47

Table S-4 Estimated crystal sizes and lattice strains from the XRD of $TiOSO_4$ studied in H_2SO_4 electrolyte

Peak	Anodic Ageing in H_2SO_4		30-min Cathodic Reactivation in H_2SO_4	
	Crystal Size (nm)	Lattice Strain (%)	Crystal Size (nm)	Lattice Strain (%)
13.84	89	1.68	79	1.51
22.80	101	0.97	112	1.05
26.63	116	1.32	102	1.01
27.61	95	0.69	101	0.81
Mean	100	1.16	98	1.01
Error	11	0.42	14	0.30

S-5. Charge Carrier Density and Flat Band Potential by Mott-Schottky Method

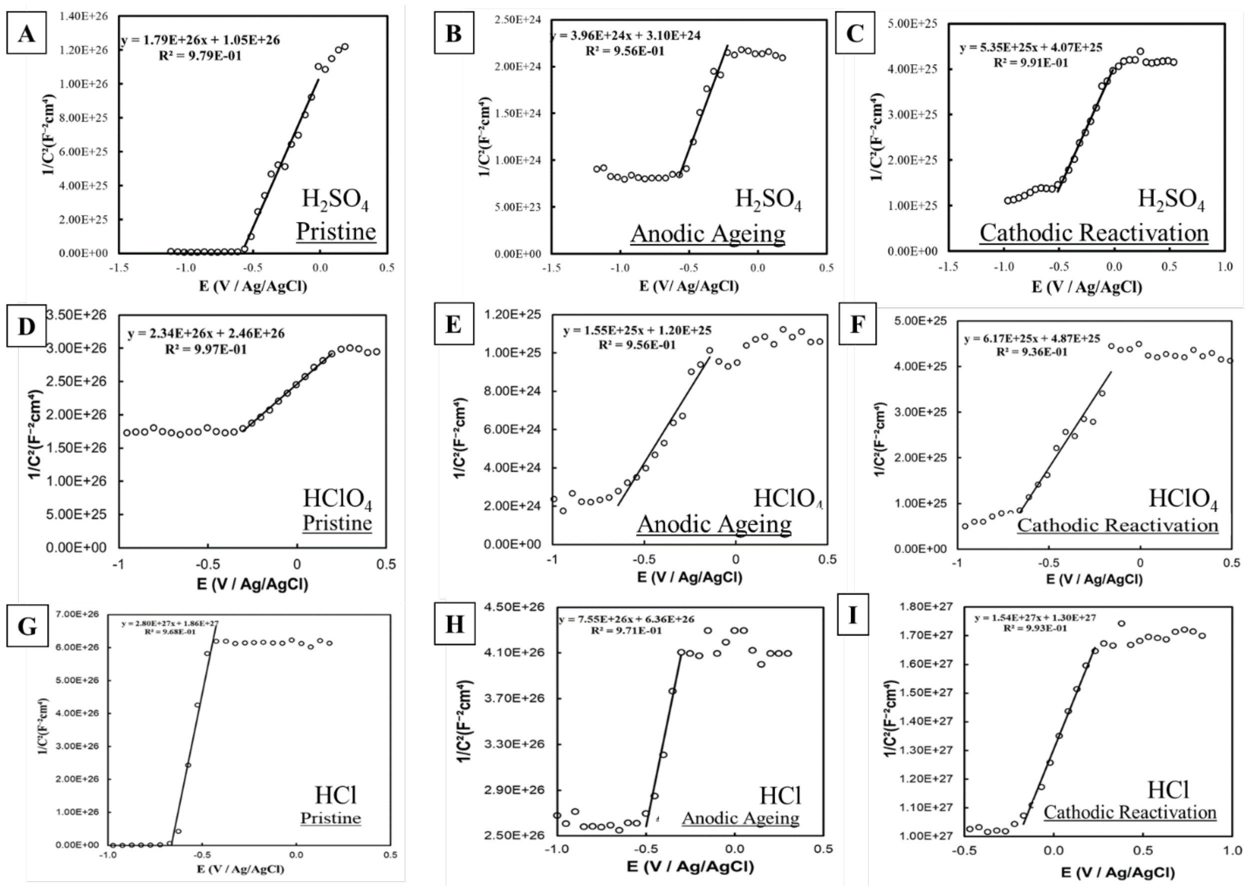

Figure S-4 Summary of Mott Schottky results of Ti_nO_{2n-1} at different states in (A)-(C) 1 M H_2SO_4, (D)-(F) 2 M $HClO_4$, and (G)-(I) 2 M HCl electrolytes. Hollow symbols and solid lines represent experimental and regression fits, respectively.

S-6. Film Resistivity by Two-Point Probe Method

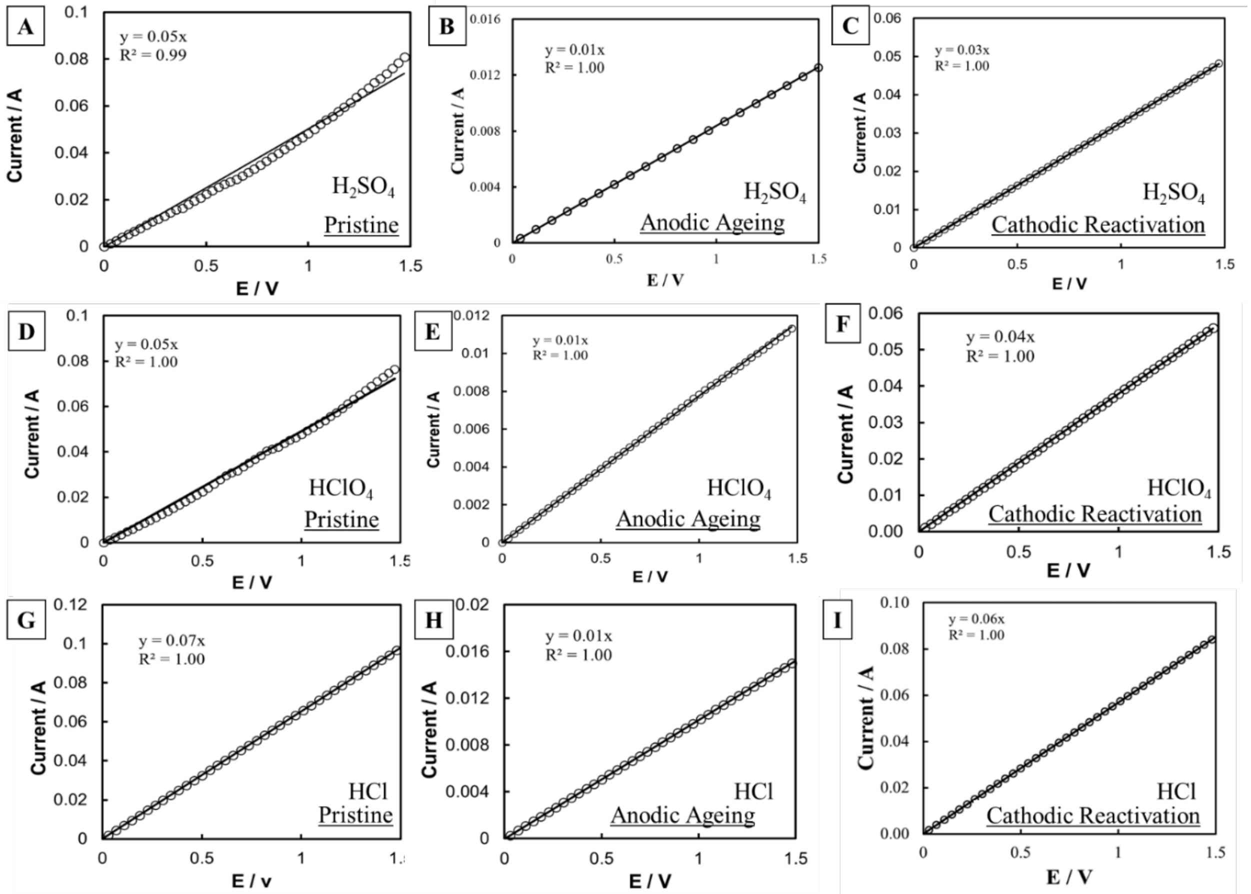

Figure S-5 Summary of film resistivities of Ti_nO_{2n-1} at different states in (A)-(C) 1 M H_2SO_4, (D)-(F) 2 M $HClO_4$, and (G)-(I) 2 M HCl electrolytes. Hollow symbols and solid lines represent experimental and regression fits, respectively.

S-7. XRD Patterns of Control Samples at Open Circuit Potential in Various Electrolytes

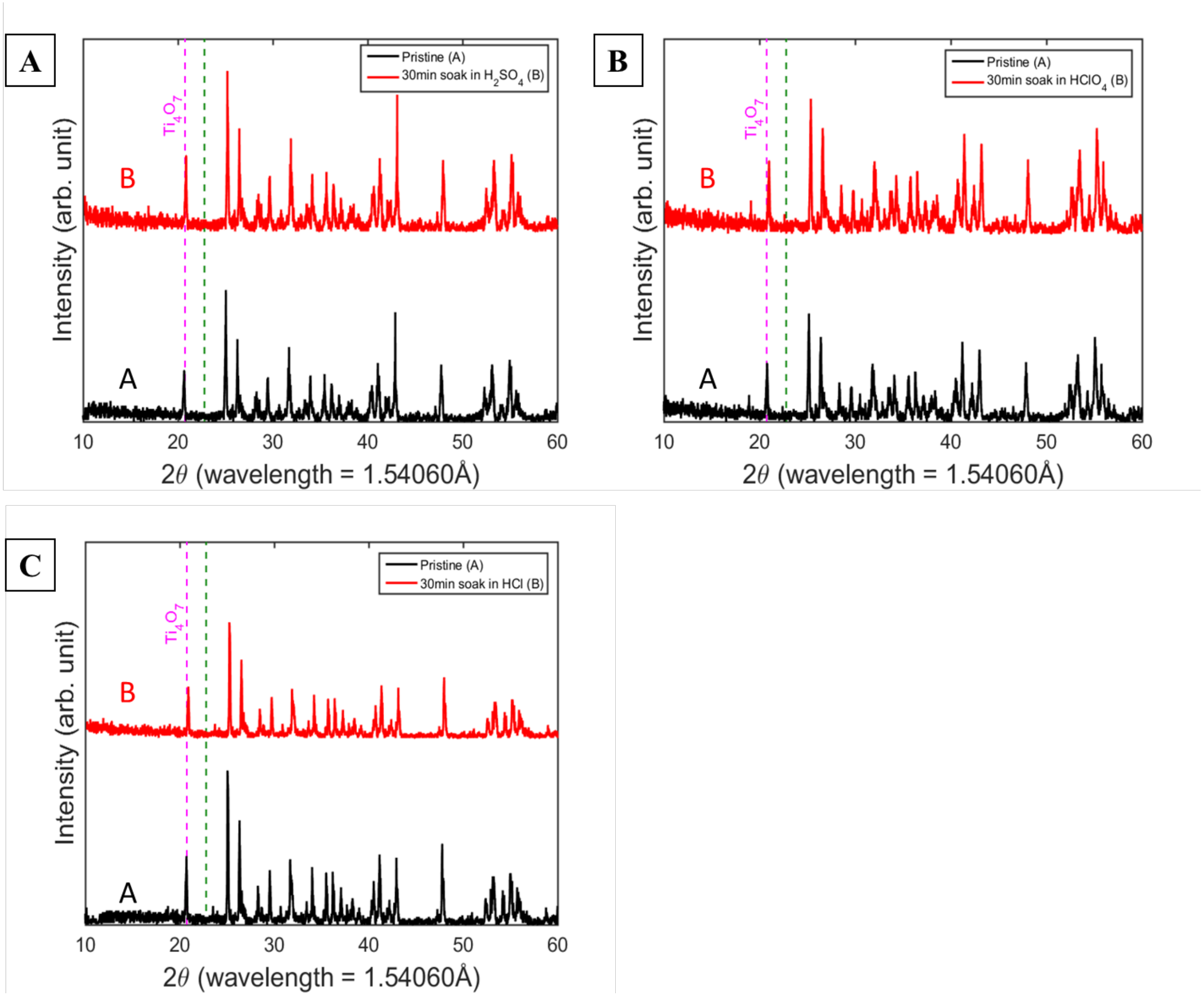

Figure S-6 XRD patterns of control samples at open circuit potential in (A) 1 M H_2SO_4, (B) 2 M $HClO_4$, and (C) 2 M HCl. 2θ angle positions at 20.78° and 22.80° are shown as pink and green vertical dashed line, respectively.

S-8. Electrochemical Impedance Spectroscopy of Ti_nO_{2n-1} at Different States

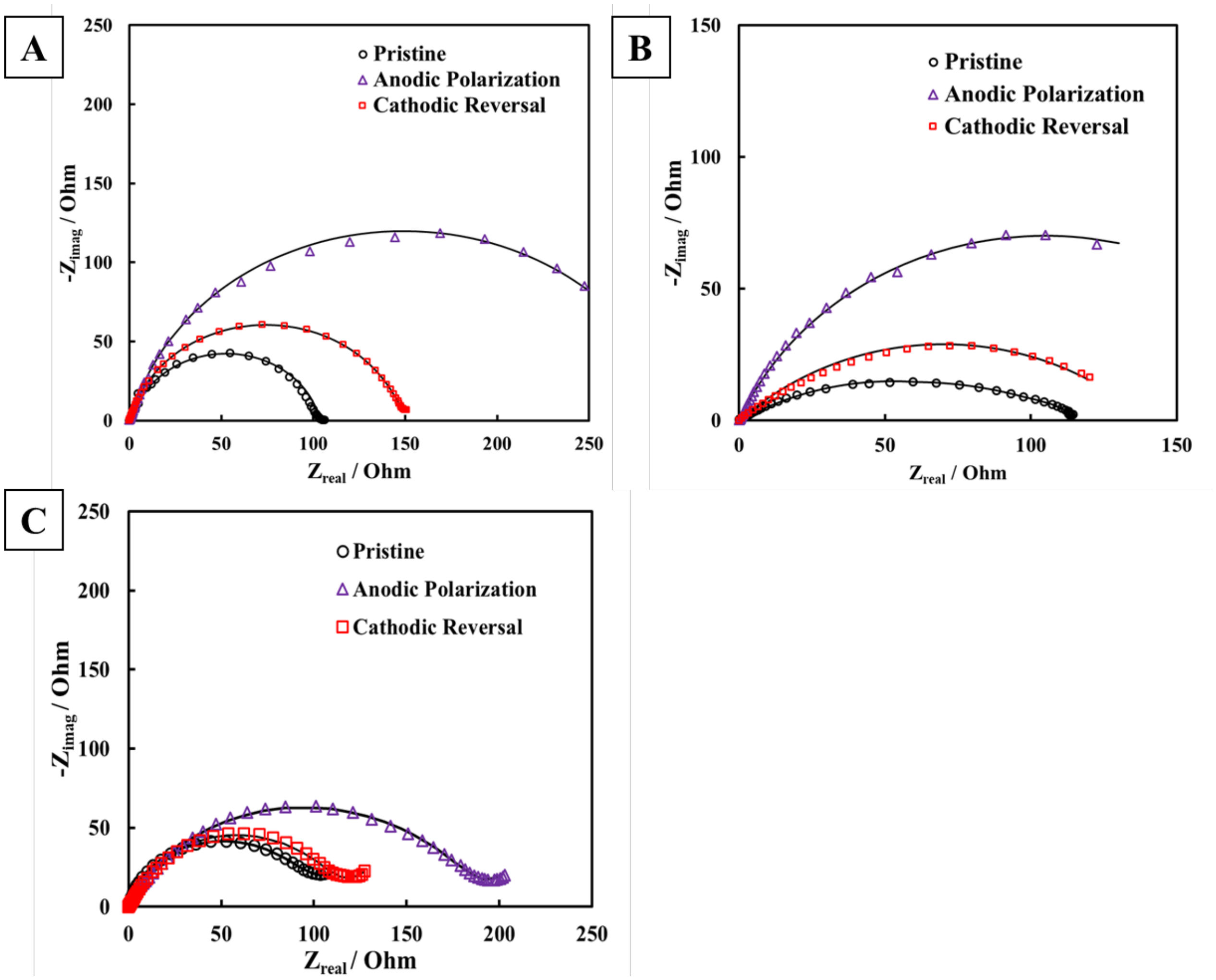

Figure S-7 Electrochemical impedance spectroscopy of Ti_nO_{2n-1} at different states in (A) 1 M H_2SO_4, (B) 2 M $HClO_4$, and (C) 2 M HCl. Hollow symbols and solid lines represent experimental and simulation data, respectively.

Table S-5 Summary of charge carrier density (N_D), flat band potential (E_{fb}), film resistivities, and charge transfer resistances (R_{ct}) of Ti_nO_{2n-1} at different states. Errors represent 95% confidence interval.

State	Physical Parameter	H_2SO_4	$HClO_4$	HCl
Pristine	N_D / cm^{-3}	$1.79\times10^{26} \pm 1.23\times10^{23}$	$2.34\times10^{26} \pm 8.79\times10^{22}$	$2.80\times10^{27} \pm 8.47\times10^{23}$
	E_{fb} / V	-0.59 ± 0.017	-0.61 ± 0.007	-0.66 ± 0.012
	Resistivity / Ω cm	18.67 ± 0.020	22.72 ± 0.002	17.13 ± 0.001
	R_{ct} / Ω	101.96 ± 5.15	105.43 ± 2.22	95.01 ± 0.21
Anodic Ageing	N_D / cm^{-3}	$3.96\times10^{24} \pm 4.11\times10^{22}$	$1.55\times10^{25} \pm 6.29\times10^{23}$	$7.55\times10^{26} \pm 5.34\times10^{24}$
	E_{fb} / V	-0.75 ± 0.034	-0.78 ± 0.041	-0.84 ± 0.021
	Resistivity / Ω cm	132.70 ± 0.004	143.59 ± 0.001	110.89 ± 0.003
	R_{ct} / Ω	296.14 ± 1.58	214.62 ± 1.15	188.39 ± 2.06
Cathodic Reactivation	N_D / cm^{-3}	$5.35\times10^{25} \pm 3.87\times10^{22}$	$6.17\times10^{25} \pm 6.33\times10^{23}$	$1.54\times10^{27} \pm 6.89\times10^{23}$
	E_{fb} / V	-0.76 ± 0.009	-0.79 ± 0.049	-0.84 ± 0.008
	Resistivity / Ω cm	33.94 ± 0.001	29.47 ± 0.004	19.72 ± 0.003
	R_{ct} / Ω	147.04 ± 0.22	139.61 ± 3.13	112.22 ± 0.70

S-9. Laser Marked Pattern Examined by Profilometer and SECM

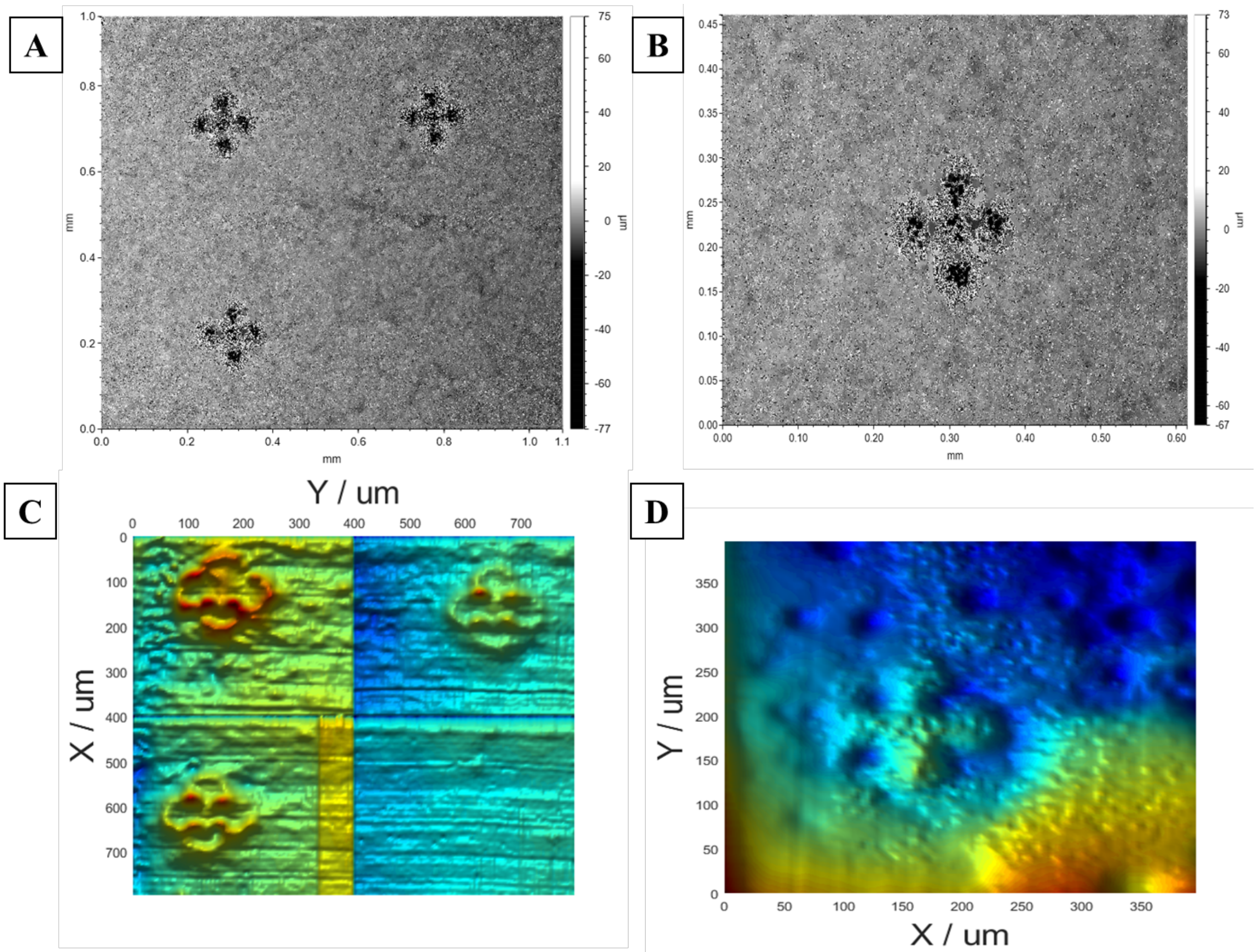

Figure S-8 Laser marked patterns shown in (A) overview by profilometer, (B) single view by profilometer, (C) overview by SECM (RuHex reduction), (D) single view by SECM (oxygen reduction reaction)

S-10. SECM Imaging and Kinetics in 1 M H_2SO_4 Electrolyte

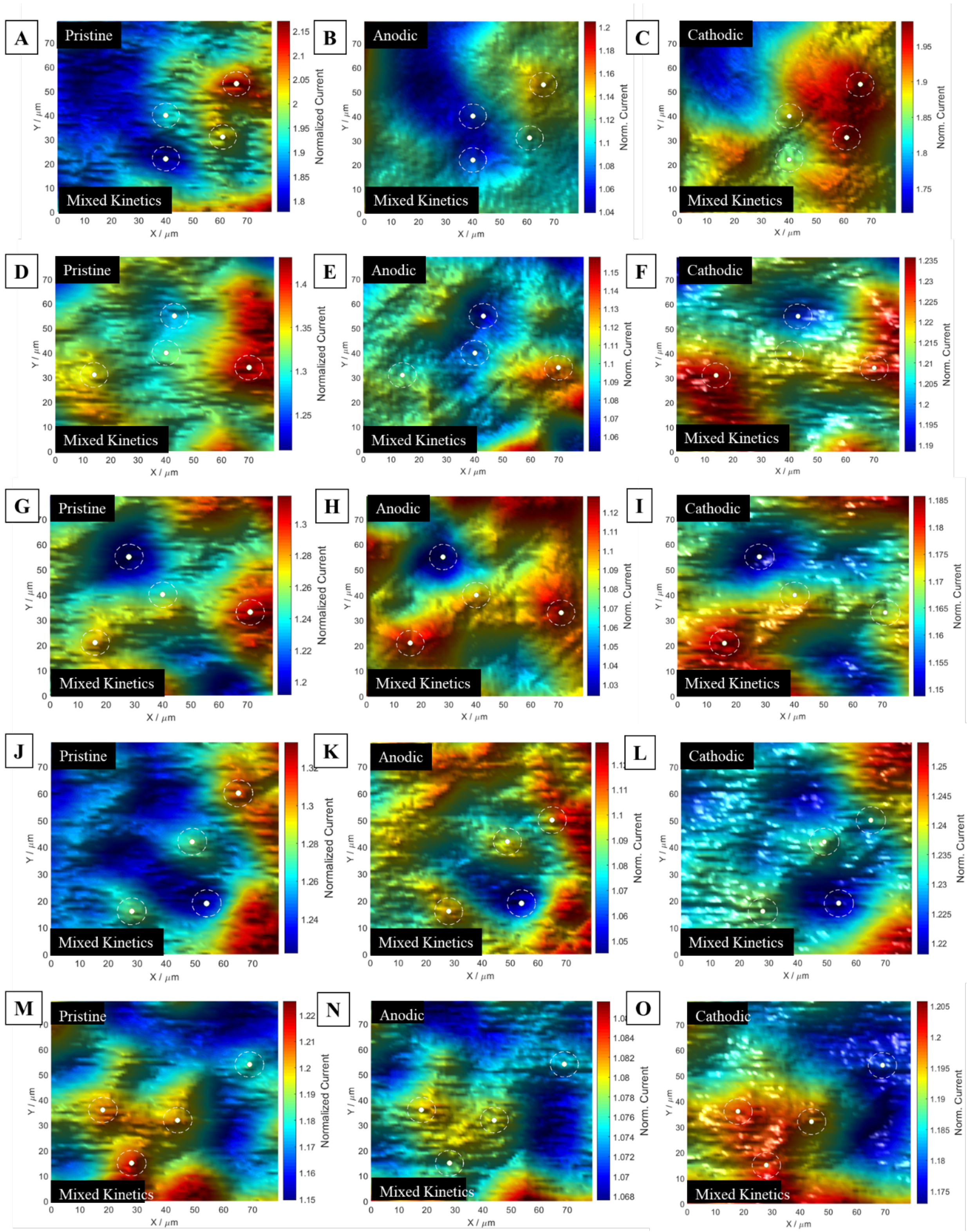

Figure S-9 SECM Images of Ti_nO_{2n-1} at different states in 1 M H_2SO_4 electrolyte at (A)-(C) area 1, (D)-(F) area 2, (G)-(I) area 3, (J)-(L) area 4, and (M)-(O) area 5.

S-11. SECM Imaging and Kinetics in 2 M $HClO_4$ Electrolyte

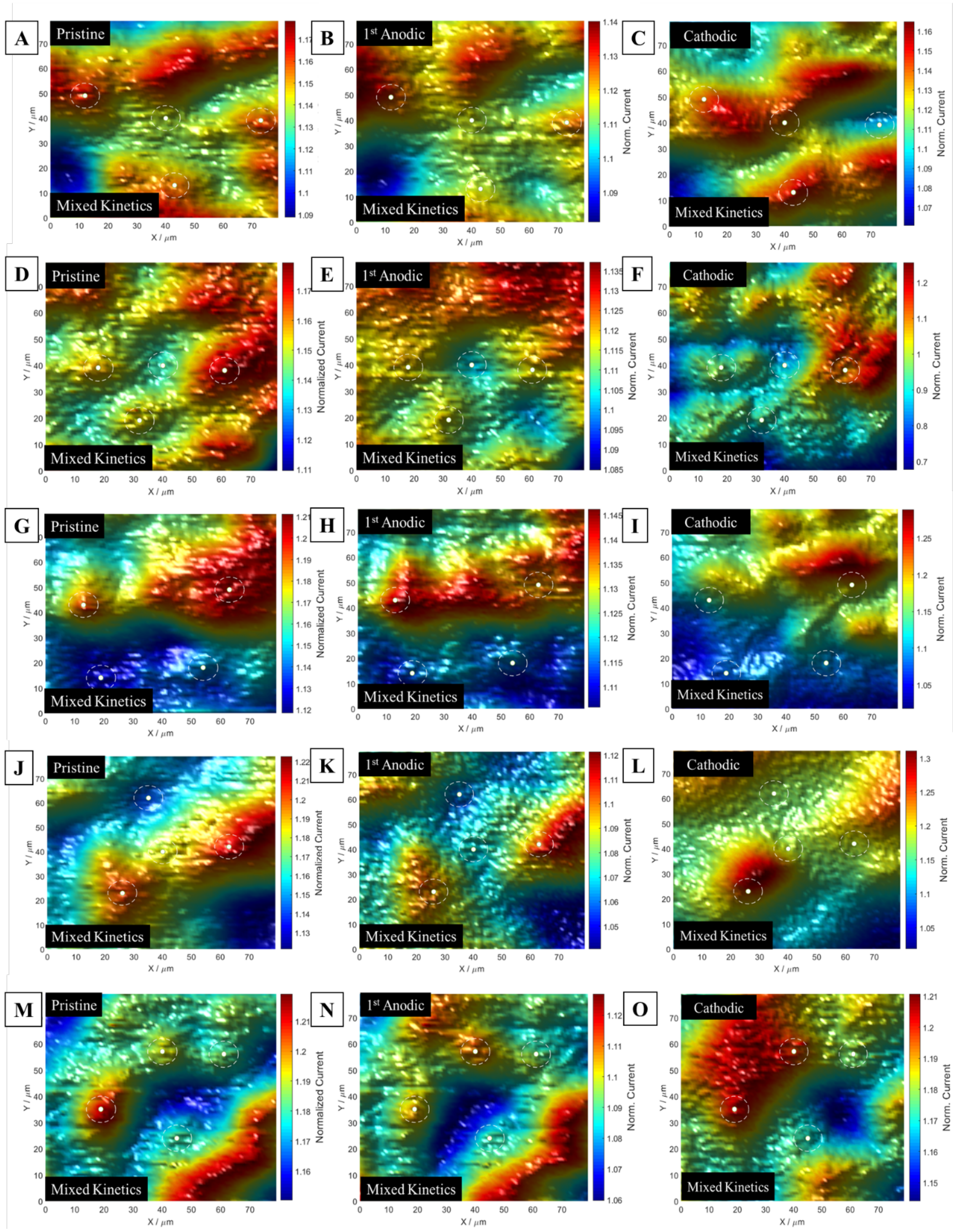

Figure S-10 SECM Images of Ti_nO_{2n-1} at different states in 2 M $HClO_4$ electrolyte at (A)-(C) area 1, (D)-(F) area 2, (G)-(I) area 3, (J)-(L) area 4, and (M)-(O) area 5.

S-12. SECM Imaging and Kinetics in 2 M HCl Electrolyte

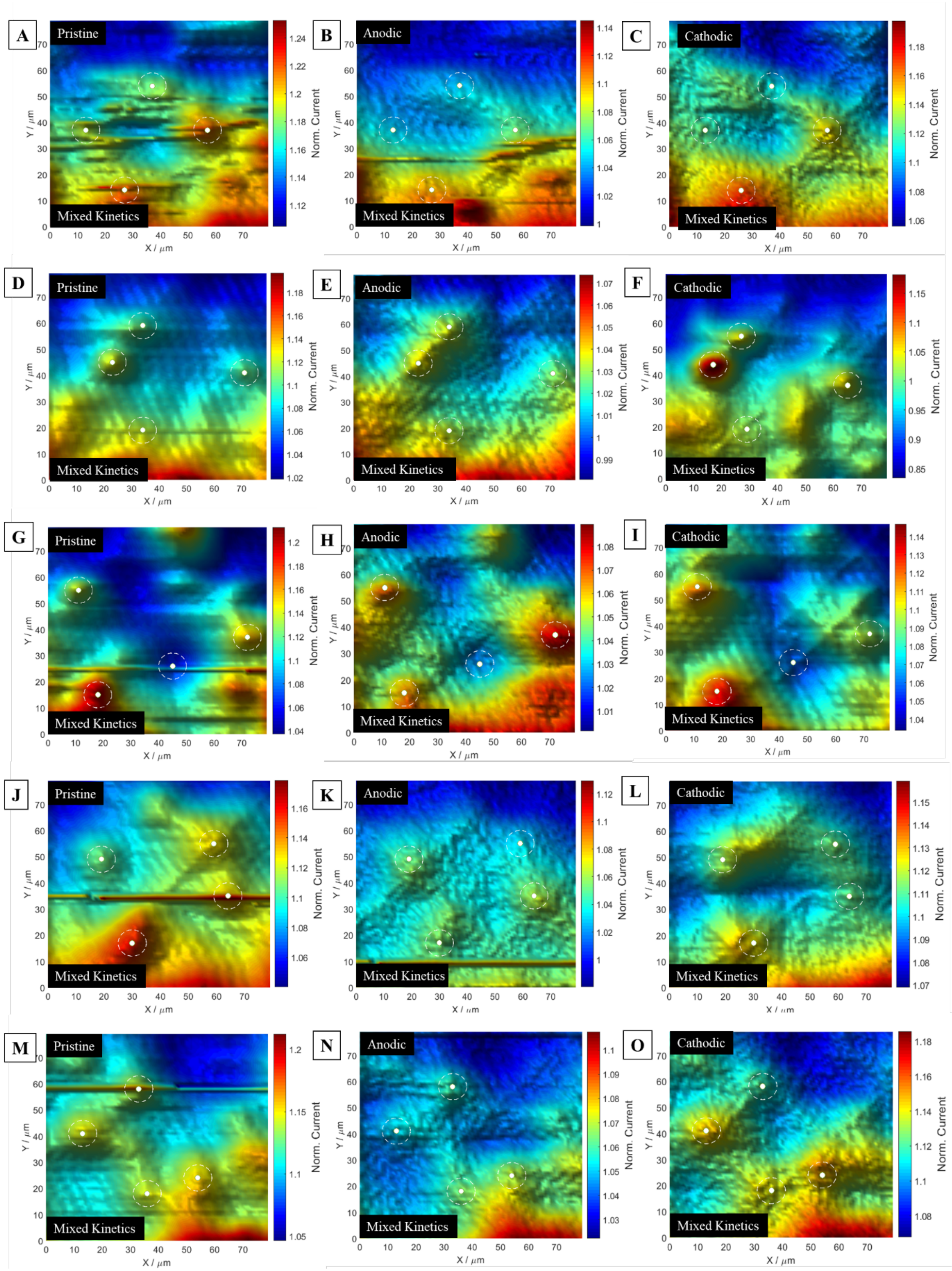

Figure 11 SECM Images of Ti_nO_{2n-1} at different states in 2 M HCl electrolyte at (A)-(C) area 1, (D)-(F) area 2, (G)-(I) area 3, (J)-(L) area 4, and (M)-(O) area 5.

S-13. Simulation of Probe Approach Curve to Resolve Localized Kinetics and Summary of Normalized First Order Rate Constants

In order to compare the local rate constants, the probe approach curves were collected at the same spot at the pristine and after anodic ageing and cathodic reactivation. The local normalized first order irreversible rate constants ($k = \frac{k_1 a}{D}$) were obtained by fitting the model shown in Equations S-1 to S-5 to the probe approach curve data.

$$\bar{I}_T(L, RG, k) = \bar{I}_T^{cond}\left(L + \frac{1}{k}, RG\right) + \frac{\bar{I}_T^{ins}(L, RG) - 1}{(1 + 2.47RG^{0.31}Lk)(1 + L^{0.006RG+0.113}k^{-0.0236RG+0.91})} \quad \text{(S-1)}$$

$$\bar{I}_T^{cond} = \alpha(RG) + \frac{1}{\beta(RG)}\frac{\pi}{4ArcTanL} + (1 - \alpha(RG) - \frac{1}{2\beta(RG)})\frac{2}{\pi}ArcTanL \quad \text{(S-2)}$$

$$\bar{I}_T^{ins} = \left[\frac{2.08}{RG^{0.358}}\left(L - \frac{0.145}{RG}\right) + 1.585\right] \times [\frac{2.08}{RG^{0.358}}(L + 0.0023RG) + 1.57 + \frac{lnRG}{L} + \frac{2}{\pi RG}\ln(1 + \frac{\pi RG}{2L})]^{-1} \quad \text{(S-3)}$$

$$\alpha = ln2 + ln2\left(1 - \frac{2}{\pi}ArcCos\frac{1}{RG}\right) - ln2[1 - (\frac{2}{\pi}ArcCos\frac{1}{RG})^2] \quad \text{(S-4)}$$

$$\beta = 1 + 0.639\left(1 - \frac{2}{\pi}ArcCos\frac{1}{RG}\right) - 0.186[1 - (\frac{2}{\pi}ArcCos\frac{1}{RG})^2] \quad \text{(S-5)}$$

where *RG* is the glass ratio of UME, *L* is the distance between the UME tip and substrate normalized by the tip radius (5 µm in this study).

For example, probe approach curves, as shown in Figure S-12B, were collected at point 1 in Figure S-12A, at the pristine, post anodic ageing and cathodic reactivation of Ti_nO_{2n-1}. The fitting of Equations S1 – S5 to experimental data yielded the normalized first order rate constants of 1.22 ± 0.0085 (pristine), 1.04 ± 0.0083 (anodic ageing), and 1.23 ± 0.0013 (cathodic reactivation).

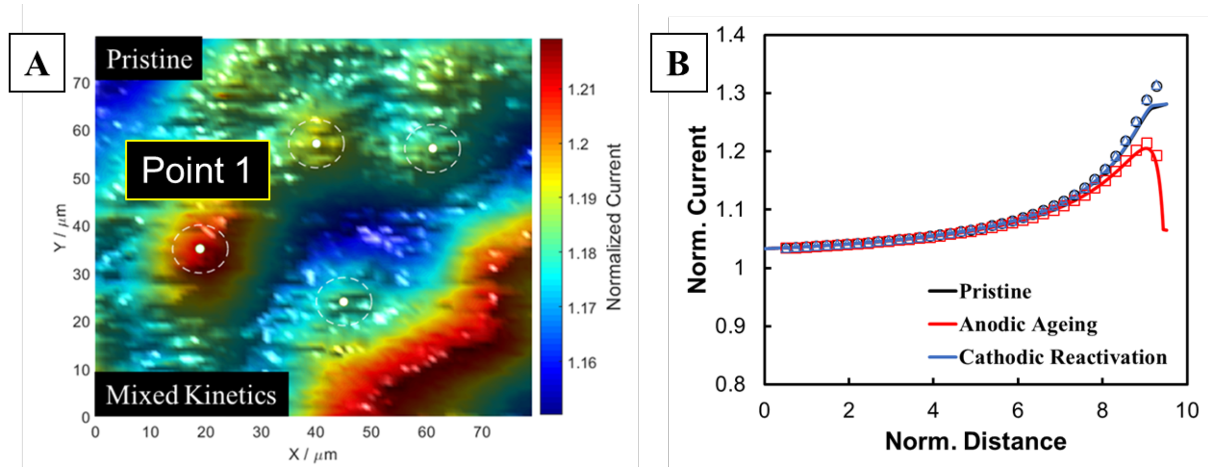

Figure S-12 (A) Image collected in 5 mM Ru[III]Hex in 100 mM KCl by SECM, and (B) probe approach curve collected at point 1 at pristine and after anodic ageing and cathodic reactivation. Solid lines and hollow points represent experimental data and simulation, respectively.

Table S-6 Summary of normalized first order rate constants of Ti_nO_{2n-1} in 1 M H_2SO_4 electrolyte

Area	Spot	H_2SO_4		
		Pristine	**Anodic**	**Cathodic**
1	40,22	1.22±0.0034	0.67±0.0021	1.17±0.0027
	40,40	1.53±0.0013	0.71±0.0011	1.49±0.0020
	61,31	1.45±0.012	0.77±0.019	1.51±0.013
	66,53	1.66±0.0019	1.22±0.010	1.51±0.0084
2	14,31	1.36±0.018	0.79±0.014	1.21±0.0018
	40,40	1.53±0.011	0.66±0.0017	1.06±0.016
	43,55	1.08±0.0075	0.71±0.0069	1.01±0.0075
	70,34	1.62±0.0072	0.89±0.0039	1.19±0.0074
3	16,21	1.29±0.013	0.89±0.019	1.01±0.012
	28,55	1.22±0.0083	0.67±0.0092	0.88±0.016
	40,40	1.57±0.012	0.75±0.0090	1.12±0.0035
	71,33	1.45±0.013	0.94±0.014	0.99±0.015
4	28,16	1.36±0.0080	0.98±0.0050	1.23±0.013
	49,42	1.62±0.0034	1.31±0.0076	1.49±0.0091
	54,19	0.97±0.0075	0.82±0.018	0.99±0.0059
	65,50	1.36±0.014	1.20±0.0053	1.27±0.017
5	18,36	1.29±0.0068	1.01±0.013	1.35±0.0097
	28,15	1.11±0.0050	0.86±0.0070	1.09±0.0077
	44,32	1.66±0.010	1.01±0.019	1.30±0.013
	69,54	0.93±0.0043	0.72±0.015	0.80±0.012
Mean		1.36	0.88	1.18
Error		0.22	0.19	0.21

Table S-7 Summary of normalized first order rate constants of Ti_nO_{2n-1} in 2 M $HClO_4$ electrolyte

Area	Spot	$HClO_4$		
		Pristine	**Anodic**	**Cathodic**
1	12,49	1.32±0.0013	1.30±0.0067	1.33±0.024
	40,40	1.02±0.0017	0.95±0.0046	1.25±0.025
	43,13	1.36±0.0097	1.01±0.0017	1.33±0.0086
	79,39	1.30±0.0067	1.22±0.0052	0.87±0.016
2	18,39	1.17±0.0053	1.15±0.0023	1.06±0.010
	32,19	1.12±0.014	1.01±0.012	0.94±0.0093
	40,40	0.97±0.0066	0.81±0.015	0.67±0.0065
	61,38	1.08±0.017	0.83±0.0043	1.32±0.0060
3	1.24	1.24±0.0097	1.20±0.0070	1.19±0.019
	0.97	0.97±0.015	0.94±0.0084	0.87±0.011
	1.15	1.15±0.0088	1.09±0.0018	1.21±0.0082
	1.29	1.29±0.017	0.99±0.0010	1.41±0.0043
4	26,23	1.11±0.010	1.02±0.0027	1.16±0.0021
	35,62	0.79±0.0048	0.75±0.019	0.77±0.0084
	40,40	0.65±0.015	0.33±0.017	0.51±0.017
	63,42	1.32±0.0058	1.27±0.013	1.11±0.017
5	19,35	1.22±0.0085	1.04±0.0083	1.23±0.0013
	40,57	1.02±0.011	0.99±0.012	1.22±0.012
	45,24	1.66±0.016	1.57±0.019	1.64±0.0026
	61,56	1.02±0.0056	0.88±0.0039	1.10±0.0076
Mean		1.14	1.02	1.11
Error		0.22	0.25	0.27

Table S-8 Summary of normalized first order rate constants of Ti_nO_{2n-1} in 2 M HCl electrolyte

Area	Spot	HCl		
		Pristine	**Anodic**	**Cathodic**
1	26, 14	1.45±0.0095	1.31±0.0025	1.45±0.0074
	57, 37	1.62±0.0004	1.44±0.0004	1.65±0.015
	13, 37	1.36±0.0009	1.25±0.0018	1.30±0.011
	37, 54	1.05±0.0026	0.61±0.0050	0.97±0.018
2	23, 45	2.09±0.0023	1.79±0.0043	1.97±0.012
	34, 19	1.05±0.0086	0.48±0.0040	0.83±0.0030
	34, 59	1.66±0.0072	1.47±0.0031	1.72±0.0030
	71, 41	1.29±0.0001	1.10±0.0051	1.26±0.0081
3	18, 15	1.66±0.0014	1.44±0.0098	1.61±0.0097
	11, 55	1.11±0.0057	0.98±0.0017	0.99±0.015
	45, 26	0.79±0.0051	0.59±0.0015	0.66±0.0071
	72, 37	1.24±0.0027	0.96±0.0035	1.26±0.0074
4	64, 35	1.40±0.0081	1.28±0.0019	1.31±0.0033
	30, 17	1.40±0.0006	1.33±0.0098	1.43±0.011
	19, 49	1.22±0.0058	1.08±0.0078	1.17±0.0064
	59, 55	1.05±0.0005	0.66±0.0063	1.06±0.0032
5	33, 58	1.66±0.0035	1.42±0.0018	1.66±0.0064
	36, 18	1.48±0.0067	1.33±0.0052	1.39±0.013
	54, 24	1.48±0.0037	1.45±0.0100	1.31±0.020
	13, 41	1.48±0.0053	0.79±0.0020	1.25±0.013
Mean		1.37	1.15	1.32
Error		0.29	0.34	0.32

S-14. Topographic Imaging by Oxygen Reduction Reaction in SECM

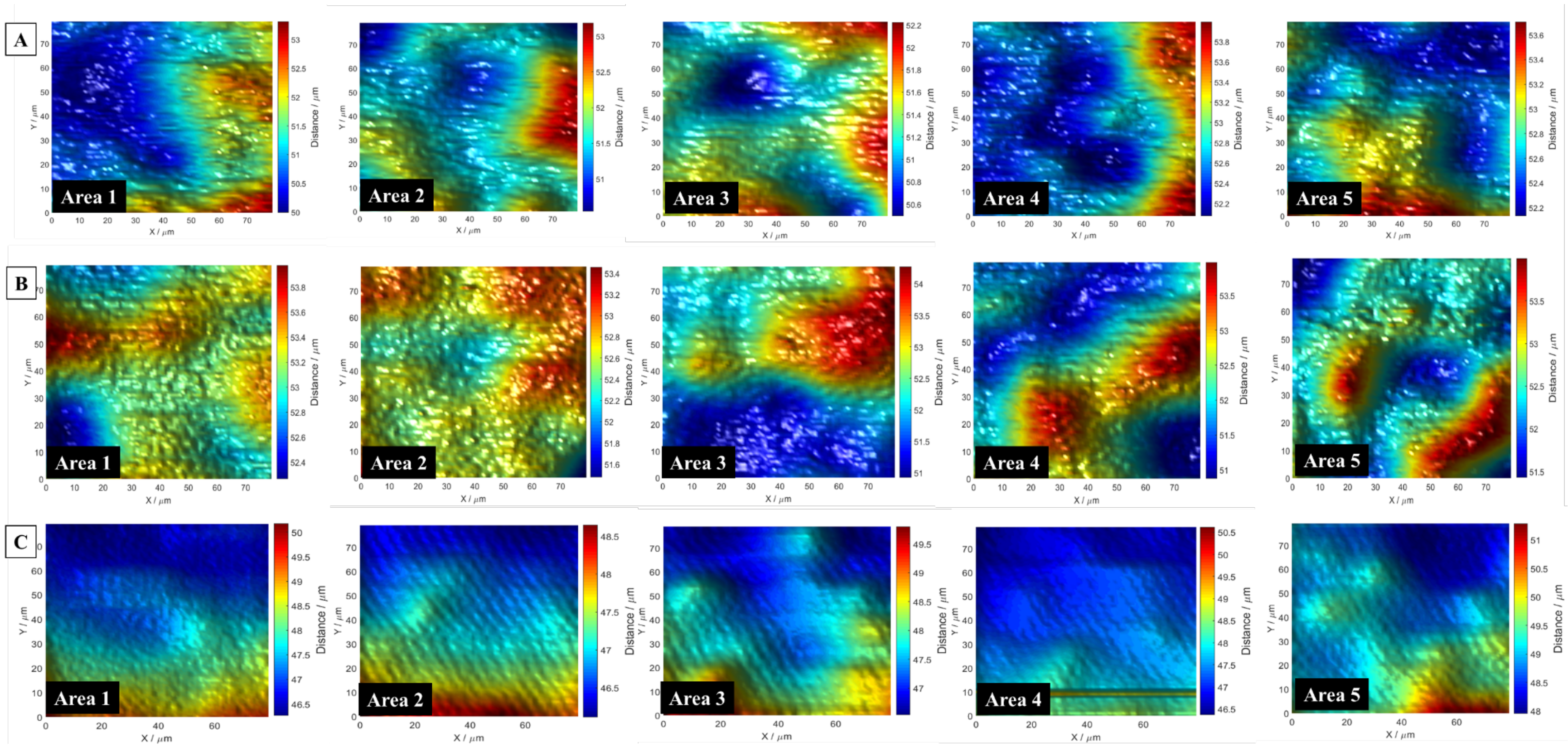

Figure S-13 Topographic images collected by oxygen reduction reaction in SECM for Ti_nO_{2n-1} samples studied in (A) H_2SO_4, (B) $HClO_4$, and (C) HCl electrolytes.

S-15. Kinetic Mapping in 1 M H_2SO_4 Electrolyte

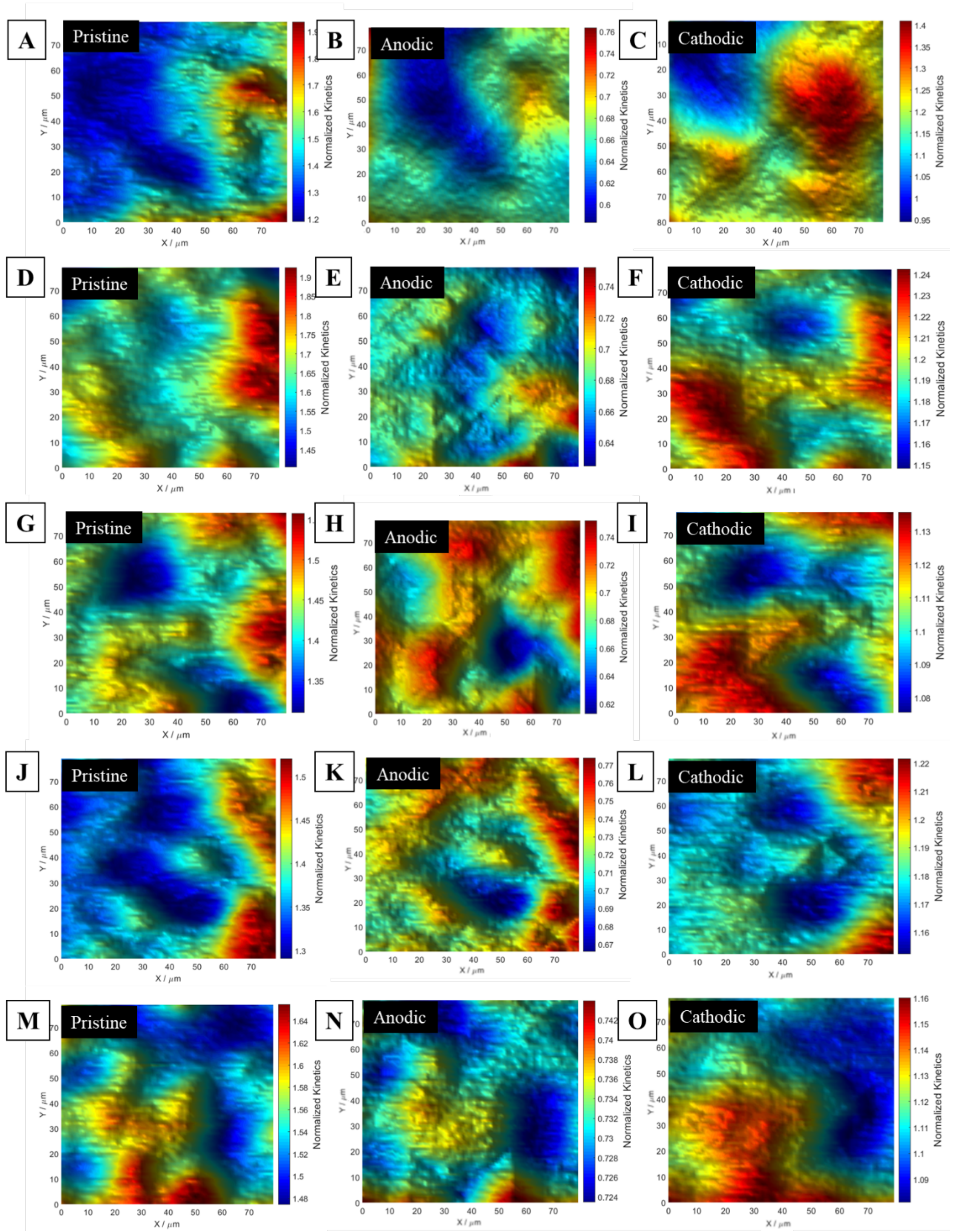

Figure S-14 Kinetic mapping of Ti_nO_{2n-1} at different states in 1 M H_2SO_4 electrolyte at (A)-(C) area 1, (D)-(F) area 2, (G)-(I) area 3, (J)-(L) area 4, and (M)-(O) area 5.

S-16. Kinetic Mapping in 2 M $HClO_4$ Electrolyte

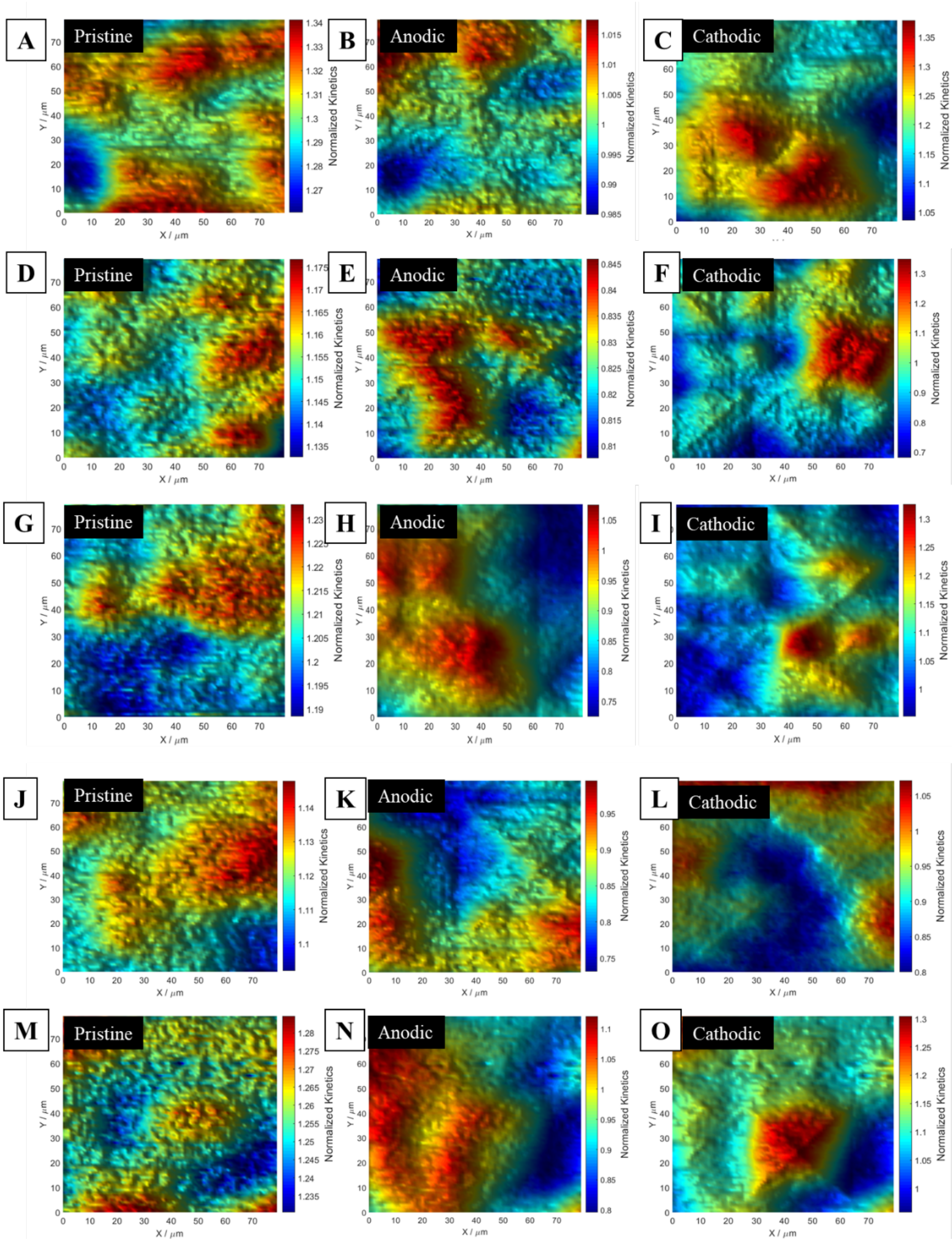

Figure S-15 Kinetic mapping of Ti_nO_{2n-1} at different states in 2 M $HClO_4$ electrolyte at (A)-(C) area 1, (D)-(F) area 2, (G)-(I) area 3, (J)-(L) area 4, and (M)-(O) area 5.

S-17. Kinetic Mapping in 2 M HCl Electrolyte

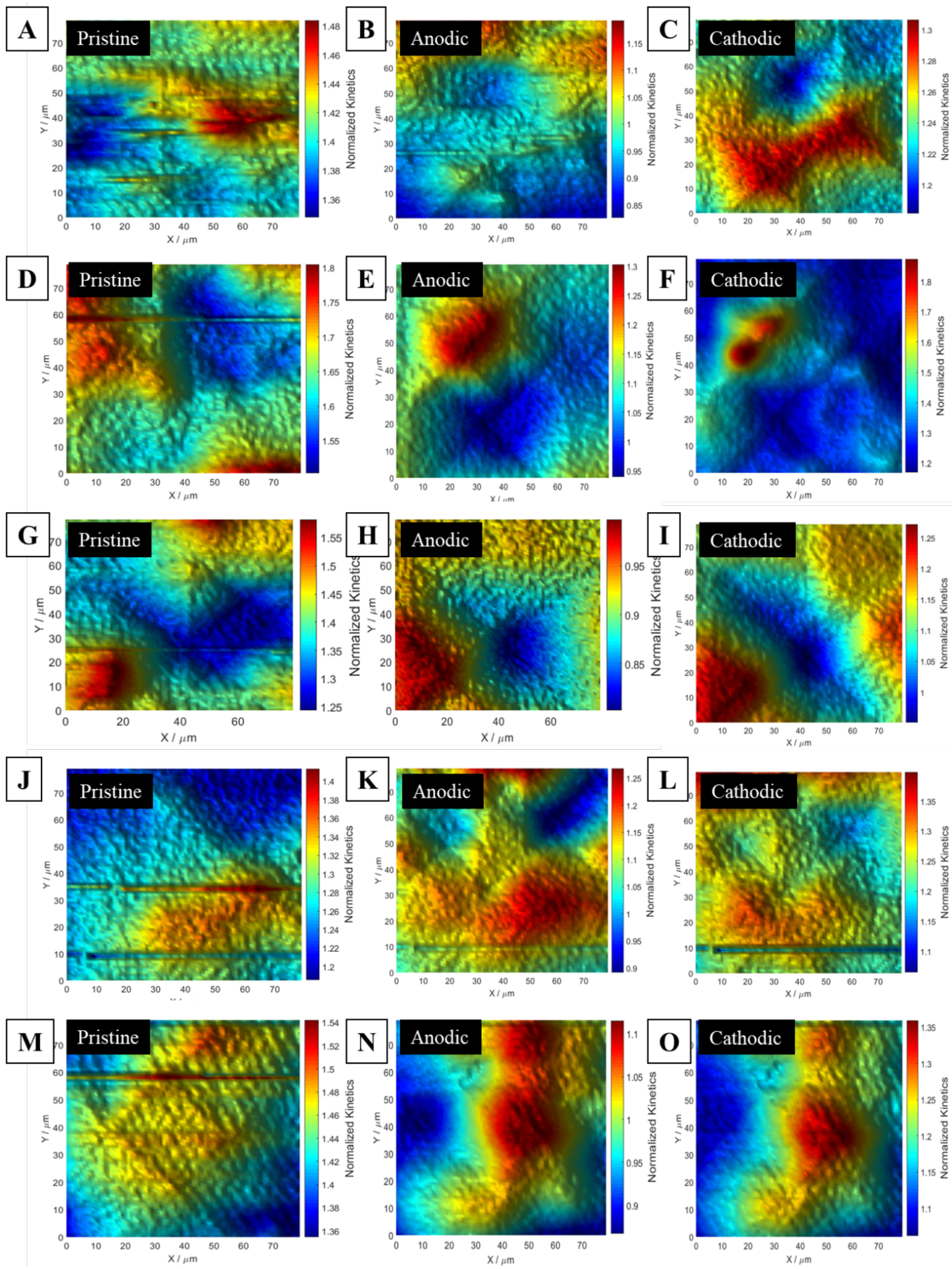

Figure S-16 Kinetic mapping of Ti_nO_{2n-1} at different states in 2 M HCl electrolyte at (A)-(C) area 1, (D)-(F) area 2, (G)-(I) area 3, (J)-(L) area 4, and (M)-(O) area 5.

S-18. Normalized First Order Rate Constants from Kinetic Mapping

Table S-9 Summary of normalized first order rate constants of Ti_nO_{2n-1} from kinetic mapping in 1 M H_2SO_4 electrolyte

Area	Spot	H_2SO_4		
		Pristine	**Anodic**	**Cathodic**
1	40,22	1.220	0.631	1.150
	40,40	1.424	0.616	1.299
	61,31	1.656	0.682	1.361
	66,53	1.888	0.706	1.376
2	14,31	1.718	0.676	1.231
	40,40	1.624	0.650	1.191
	43,55	1.549	0.637	1.157
	70,34	1.817	0.738	1.213
3	16,21	1.484	0.721	1.132
	28,55	1.317	0.710	1.076
	40,40	1.416	0.707	1.113
	71,33	1.527	0.686	1.006
4	28,16	1.404	0.746	1.185
	49,42	1.390	0.749	1.186
	54,19	1.299	0.702	1.158
	65,50	1.427	0.762	1.179
5	18,36	1.599	0.737	1.143
	28,15	1.626	0.732	1.145
	44,32	1.605	0.736	1.140
	69,54	1.593	0.731	1.095

Table S-10 Summary of normalized first order rate constants of Ti_nO_{2n-1} from kinetic mapping in 2 M $HClO_4$ electrolyte

Area	Spot	$HClO_4$		
		Pristine	**Anodic**	**Cathodic**
1	12,49	1.319	1.004	1.253
	40,40	1.303	1.002	1.249
	43,13	1.321	1.000	1.378
	79,39	1.316	1.005	1.043
2	18,39	1.159	0.840	0.966
	32,19	1.149	0.844	0.947
	40,40	1.153	0.822	0.786
	61,38	1.163	0.829	1.282
3	1.24	1.228	0.952	1.051
	0.97	1.191	0.928	0.971
	1.15	1.205	0.959	1.188
	1.29	1.225	0.800	1.175
4	26,23	1.128	0.924	0.928
	35,62	1.119	0.759	0.890
	40,40	1.129	0.785	0.802
	63,42	1.133	0.854	0.923
5	19,35	1.244	1.014	1.111
	40,57	1.255	0.960	1.129
	45,24	1.258	0.991	1.304
	61,56	1.258	0.851	1.086

Table S-11 Summary of normalized first order rate constants of Ti_nO_{2n-1} from kinetic mapping in 2 M HCl electrolyte

Area	Spot	HCl		
		Pristine	**Anodic**	**Cathodic**
1	26, 14	1.421	1.018	1.306
	57, 37	1.474	1.042	1.294
	13, 37	1.365	0.966	1.274
	37, 54	1.433	0.905	1.182
2	23, 45	1.706	1.286	1.872
	34, 19	1.626	0.940	1.184
	34, 59	1.656	1.271	1.610
	71, 41	1.568	1.009	1.237
3	18, 15	1.572	0.987	1.272
	11, 55	1.352	0.930	1.060
	45, 26	1.261	0.803	0.957
	72, 37	1.273	0.897	1.202
4	64, 35	1.389	1.185	1.215
	30, 17	1.347	1.157	1.311
	19, 49	1.268	1.028	1.211
	59, 55	1.231	0.922	1.152
5	33, 58	1.538	0.990	1.190
	36, 18	1.484	1.028	1.255
	54, 24	1.444	1.031	1.270
	13, 41	1.469	0.870	1.081

S-19. Summary of *p* Values from Welch's t-Test Performed on Rate Constant Data

Table S-12 Summary of *p* values from Welch's t test performed on rate constants when EIS data were used as the compared sample (null hypothesis: zero mean difference; α: 0.05)

Electrolyte	**Statistical Parameter**	**Anodic Ageing**		**Cathodic Reactivation**	
		Approach Curve (N = 20)	**Kinetic Mapping (N = 32000)**	**Approach Curve (N = 20)**	**Kinetic Mapping (N = 32000)**
H_2SO_4	p	1.9×10^{-9}	0.22	1.2×10^{-4}	0.20
	t	2.07	3.18	2.16	3.18
	d.f.	22	3	13	3
$HClO_4$	p	5.5×10^{-7}	0.11	2.5×10^{-6}	0.09
	t	2.09	3.18	2.20	3.18
	d.f.	20	3	11	3
HCl	p	8.6×10^{-7}	0.11	1.9×10^{-7}	0.10
	t	2.09	3.18	2.08	3.18
	d.f.	20	3	21	3

S-20. Charge Carrier Density and Flat Band Potential by Mott-Schottky Method on Various Magnéli Phases

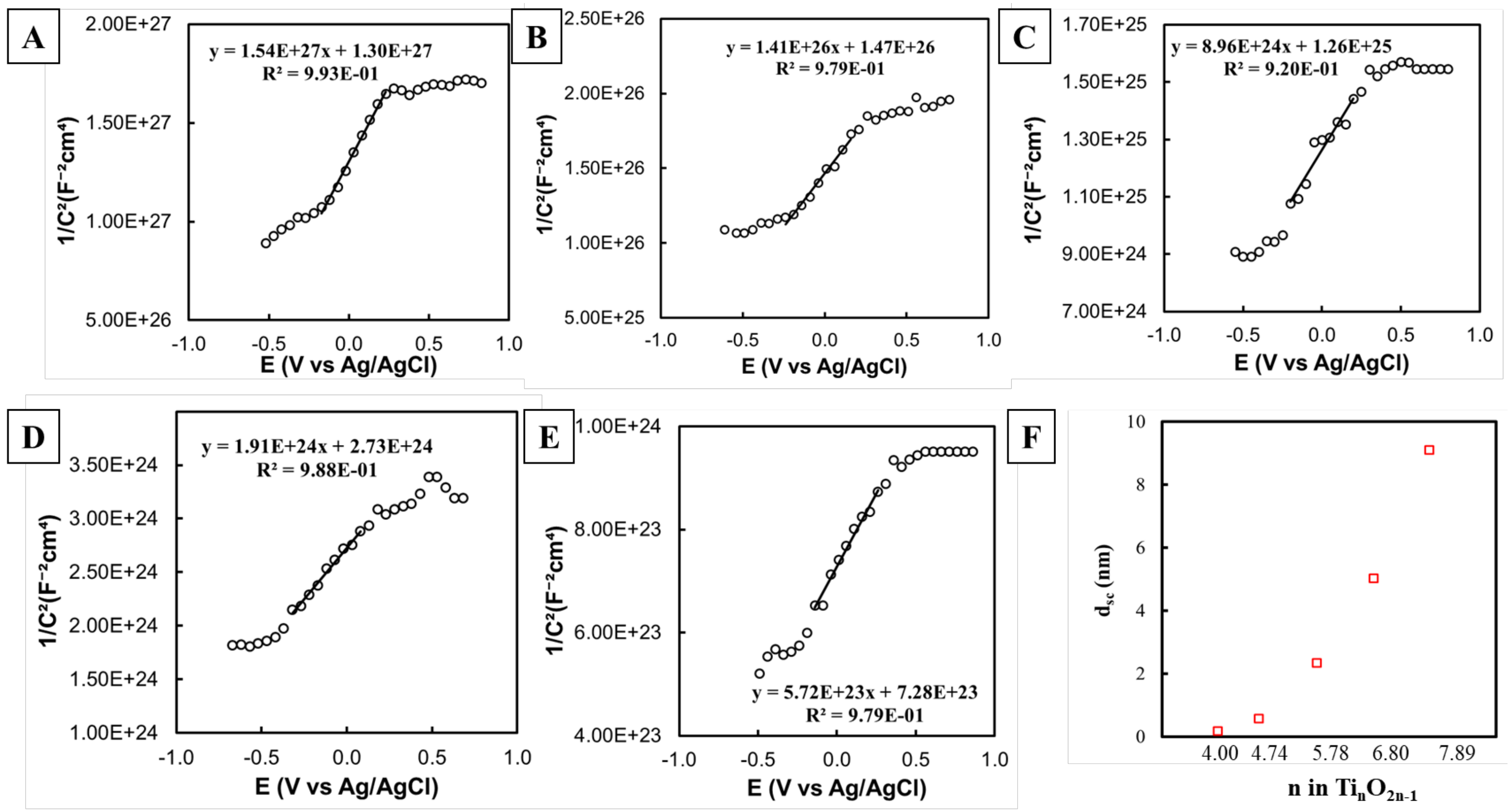

Figure S-17 Summary of Mott-Schottky results of Ti_nO_{2n-1} with value of n at (A) 4.00, (B) 4.74, (C) 5.78, (D) 6.80, and (E) 7.89, respectively. (F) Calculated space charge layer thickness of different Ti_nO_{2n-1} samples.

Table S-13 Summary of charge carrier densities (N_D), flat band potential (E_{fb}) and space charge layer thickness (d_{sc}) of Ti_nO_{2n-1}.

***n* in Ti_nO_{2n-1}**	**N_D / cm^{-3}**	**E_{fb} / V**	**d_{sc} / nm**
4.00	$1.54\times10^{27} \pm 1.31\times10^{25}$	-0.84 ± 0.03	0.17
4.74	$1.41\times10^{26} \pm 3.82\times10^{25}$	-1.04 ± 0.05	0.56
5.78	$8.96\times10^{24} \pm 7.23\times10^{22}$	-1.41 ± 0.21	2.3
6.80	$1.91\times10^{24} \pm 5.94\times10^{22}$	-1.35 ± 0.14	5.0
7.89	$5.72\times10^{23} \pm 1.77\times10^{21}$	-1.27 ± 0.09	9.1

S-21. Thermogravimetric Analysis

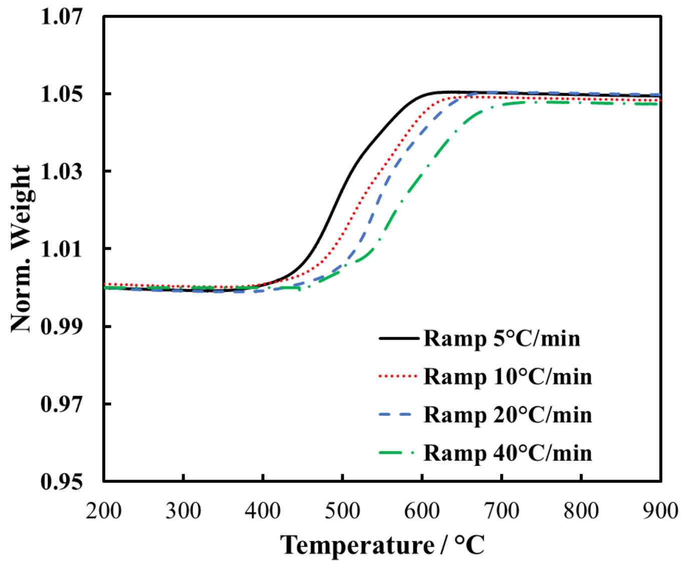

Figure S-18 Thermogravimetric analysis results of Ti_nO_{2n-1} in air at different temperature ramps

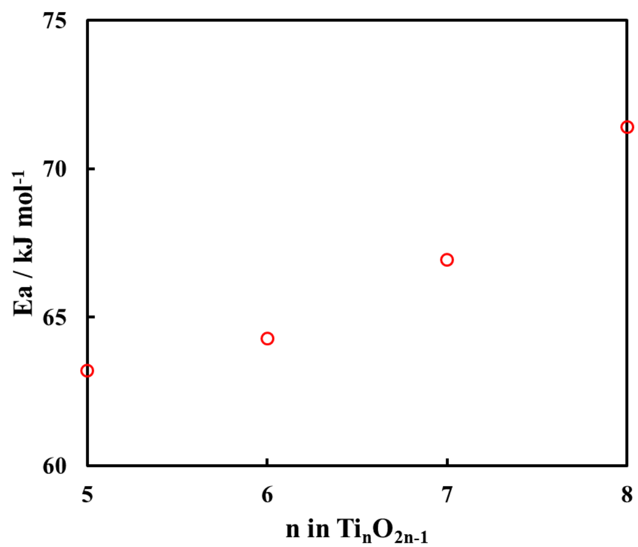

Figure S-19 Activation energy (E_a) required for the conversion from Ti_4O_7 to Ti_nO_{2n-1} (n >4)

S-22. Voltammetry of Ti_nO_{2n-1} in Acidic Electrolytes

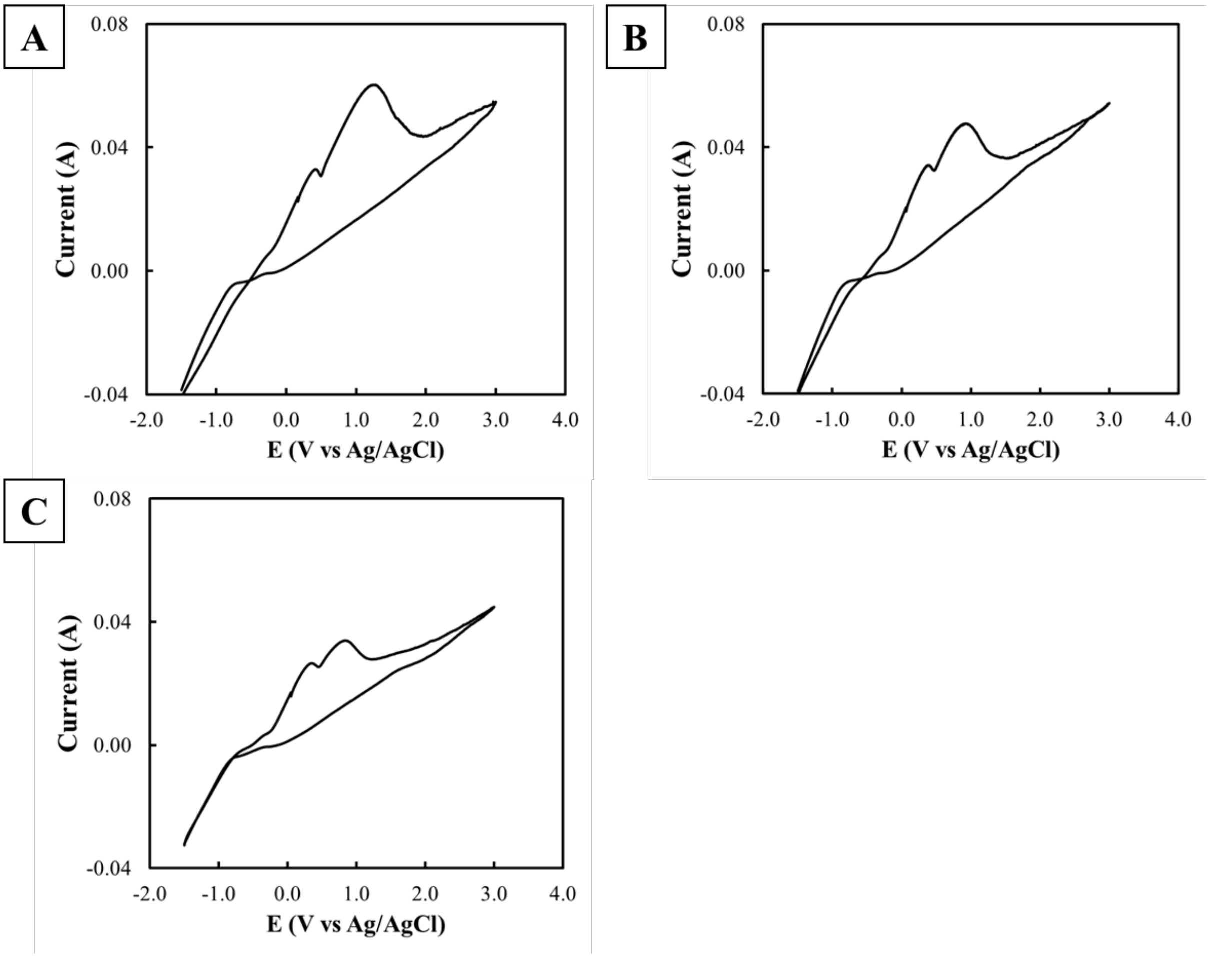

Figure S-20 Cyclic voltammograms on Ti_nO_{2n-1} in 1 M H_2SO_4, 2 M $HClO_4$, and 2 M HCl.

S-23. Peak Significance in the XPS Spectra

In Figure 6A of the main text, S 2p peak is observed, and Figure 6B exhibits a S $2p_{3/2}$-$2p_{1/2}$ doublet with 1.1 eV splitting. A unique S 2p doublet related to sulfate species (SO_4^{2-}) with S $2p_{3/2}$ at 169.0 eV is found, while sulfite with S $2p_{3/2}$ at 167.0 eV is not present.[1] Figure 6C shows the Ti 2p spectrum, the binding energy peaks at 464.6 and 458.8 eV are associated to $2p_{1/2}$ and $2p_{3/2}$ of Ti^{4+}. The Ti $2p_{1/2}$ peak is fitted to reveal two peak energies at 464.6 and 463.1 eV. The Ti $2p_{3/2}$ can also be resolved into two Gaussian peaks at 468.8 and 457.9 eV, which can be related to the Ti^{4+} and Ti^{3+}, respectively, meanwhile, the $2p_{1/2}$ binding energy of 464.6 and 463.1 eV can be attributed to Ti^{4+} and Ti^{3+}, respectively. These resolved peaks are consistent with literature values.[2,3]

S-24. Quantum Mechanical Calculations

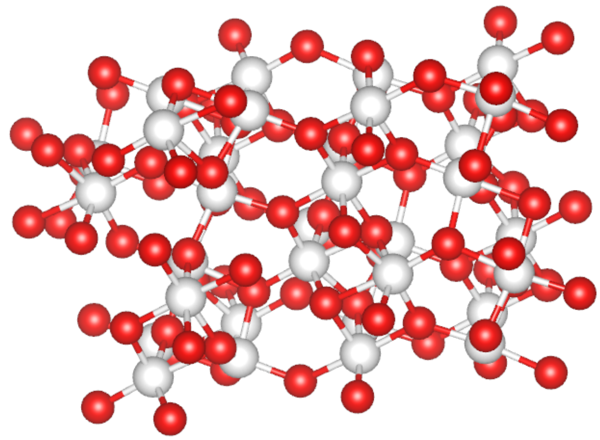

Figure S-21 Optimized structure of Ti_4O_7 (1-20) surface. Atom key:red = oxygen; grey = titanium.

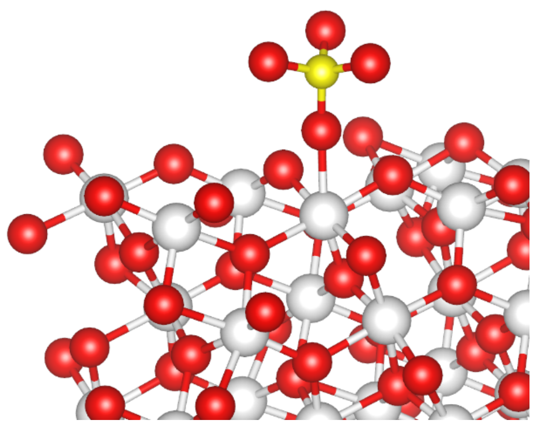

Figure S-22 Optimized structure of SO_4 adsorbed on the Ti_4O_7 (1-20) surface. Atom key: yellow = sulfur; red = oxygen; grey = titanium.

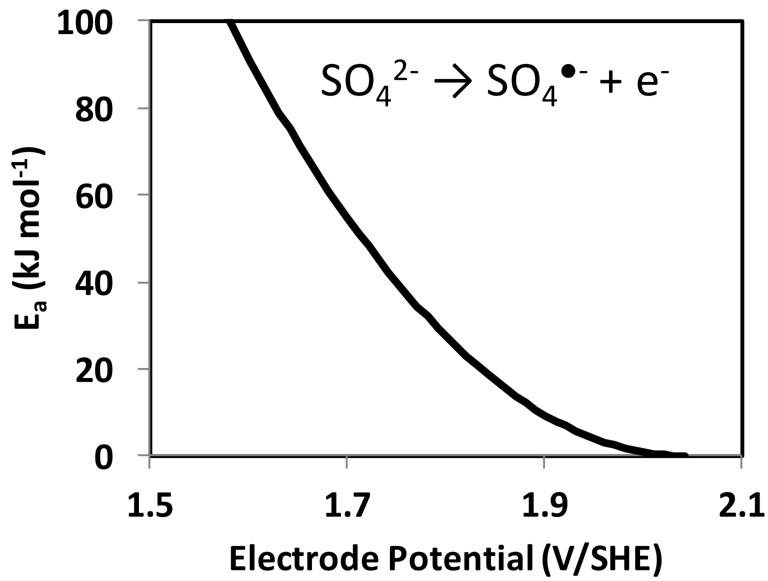

Figure S-23 DFT determined E_a vs electrode potential profile for sulfate oxidation.

The E_a vs potential profile for the oxidation of SO_4^{2-} is shown in Figure S-23 for Reaction 12 discussed in the text. The calculated electrode potential for Reaction 10 was $E^o = 2.0$ V/SHE, and reorganization energy was 5.0 kJ mol^{-1}.

References

1 N. Andreu, D. Flahaut, R. Dedryvère, M. Minvielle, H. Martinez and D. Gonbeau, *ACS Appl. Mater. Interfaces*, 2015, **7**, 6629–6636.

2 S. Pan, X. Liu, M. Guo, S. fung Yu, H. Huang, H. Fan and G. Li, *J. Mater. Chem. A*, 2015, **3**, 11437–11443.

3 P. Geng and G. Chen, *J. Memb. Sci.*, 2016, **498**, 302–314.